BLIND HYPERSPECTRAL IMAGE SUPER RESOLUTION VIA SIMULTANEOUSLY SPARSE AND TV CONSTRAINT

Changzhong Zou, Youshen Xia

College of Mathematics and Computer Science
Fuzhou University, China
(e-mail: {chzhzou,ysxia}@fzu.edu.cn)

ABSTRACT

This paper proposes a novel blind hyperspectral image super resolution method. The proposed method can estimate simultaneously the unknown hyperspectral image and the blur kernel based on the linear spectral unmixing technique. The total variation term is used for the blur kernel regularization and simultaneous total variation and sparse representation are used for abundance regularization terms. Because the image and blur kernel are simultaneously estimated with the double regularization terms introduced for abundance, the estimation error can be minimized so that the performance of the proposed method can be improved. Finally, the proposed optimization formulation is effectively solved by block coordinate descent method. Experimental results show that the proposed method is effective and superior to existing blind hyperspectral image super resolution approach in terms of reconstruction quality.

Index Terms— hyperspectral image, total variation, sparse representation, blind super resolution.

1. INTRODUCTION

Recently, hyperspectral image (HSI) has drawn attract attention due to their various applications in environment studies, military surveillance, and so on [1]. However, their spatial resolution is often lower than that of multispectral image (MSI) because of the limitation of spectral imaging techniques. Therefore, it is desirable to enhance the spatial resolution of HSI by fusing the observed low spatial resolution HSI and MSI.

Many methods for HSI super resolution have been proposed. First, the pansharpening methods had been extensively studied for HSI super resolution [2, 3]. Furthermore, based on HSI and MSI observation model, various methods were proposed in the recent years, which can be categorized into two main classes. The first class method is Bayesian statistical method, such as [4–8]. The class of linear spectral unmixing techniques as the second class method was developed. In [9], Yokoya proposed a coupled nonnegative matrix factorization approach to fuse the HSI and MSI. By considering different constraints such as nonnegativity and sparsity, several improved matrix factorization methods for HSI super resolution were presented [10–16]. Recently, Dong et al. [17] proposed the nonnegative structure sparse representation HSI super resolution method. All these methods assumed the blur kernel is known, however, in practice the blur kernel is not available. At present, Simoes et al. [18] first proposed a convex optimization method (called HySure) for hyperspectral image super resolution by total variation regularization model for HSI super resolution in the case of the unknown blur kernel. On the other hand, the HySure method separated the image and blur kernel estimation so as to accumulate image estimation error, specially in heavy noise.

In this paper, we propose a novel method for blind HSI super resolution based on linear spectral unmixing model. In the proposed method, simultaneous sparse and TV constraint terms for abundance matrix and a TV regularization term for blur kernel into a unifying optimization formulation are introduced. Because the image and blur kernel are simultaneously estimated by the double regularization terms, the estimation error can be minimized. Finally, the proposed formulation is effectively solved by block coordinate descent method. Computed results confirm that the proposed method has a better performance than existing blind HSI super resolution approach, in terms of reconstruction quality.

The rest of this paper is organized as follows. Section II introduces observed model and blind estimation method. Section III presents an optimization algorithm for blind HSI super resolution. Section IV gives the experimental results. Conclusion is given in Section V.

2. OBSERVED MODEL AND ESTIMATION

2.1. HSI observed model

We are concerned with the following HSI and MSI observation model:

$$\mathbf{Y}_h = \mathbf{YHD} + \mathbf{N}_h, \mathbf{Y}_m = \mathbf{RY} + \mathbf{N}_m, \tag{1}$$

Thanks to the National Natural Science Foundation of China under Grant No. 61473330 and Natural Science Foundation of Fujian Province under Grant No. 2017J01751 for funding.

where $\mathbf{Y} \in R^{B_h \times L_m}$ denotes the unknown high resolution HSI with spectral bands number B_h and pixels of every band L_m , $\mathbf{Y}_h \in R^{B_h \times L_h}$ and $\mathbf{Y}_m \in R^{B_m \times L_m}$ are the observed HSI and MSI, respectively, $\mathbf{R} \in R^{B_m \times B_h}$ is the spectral response, $\mathbf{D} \in R^{L_m \times L_h}$ is down-sampling matrix, $\mathbf{N}_h \in R^{B_h \times L_h}$ and $\mathbf{N}_m \in R^{B_m \times L_m}$ denote additional Gaussian noise. Our purpose is to estimate $\mathbf{Y}$ under the unknown blur kernel $\mathbf{H} \in R^{L_m \times L_m}$.

2.2. Proposed estimation method

2.2.1. *the data-fidelity with unknown blur kernel*

According to Maximization likelihood theory, the data-fidelity term is to be minimized as:

$$\min_{\mathbf{Y},\mathbf{H}} \|\mathbf{Y}_h - \mathbf{YHD}\|_F^2 + \|\mathbf{Y}_m - \mathbf{RY}\|_F^2. \tag{2}$$

Based on linear spectral unmixing technique [19], $\mathbf{Y}$ can be approximately denoted as $\mathbf{Y} = \mathbf{EA}$, where $\mathbf{E} \in R^{B_h \times P}$ and $\mathbf{A} \in R^{P \times L_m}$ denote the endmember and abundance matrix, respectively. Then (2) can be described as:

$$\min_{\mathbf{E},\mathbf{A},\mathbf{H}} \|\mathbf{Y}_h - \mathbf{EAHD}\|_F^2 + \|\mathbf{Y}_m - \mathbf{REA}\|_F^2. \tag{3}$$

Usually the endmember $\mathbf{E}$ can be estimated in advance. In our work, we estimate $\mathbf{E}$ according to VCA technique [20] based on the observed HSI. Thus (3) can be simply expressed as:

$$\min_{\mathbf{A},\mathbf{H}} \|\mathbf{Y}_h - \mathbf{EAHD}\|_F^2 + \|\mathbf{Y}_m - \mathbf{REA}\|_F^2. \tag{4}$$

Since the reconstruction problem above is ill-posed, the regularization technique should be considered.

2.2.2. *abundance regularization*

Because the neighbourhood pixels of HSI are high correlation and they contain the similar subset of the available endmembers, the corresponding vectors of abundance of the neighbourhood pixels are similar. Thus the abundance should be smooth in the spatial dimension. That is, the abundance matrix $\mathbf{A}$ should be smooth. Since total variation can efficiently express the piecewise smoothness information, the following TV term is introduced in our model:

$$\mathrm{TV}(\mathbf{A}) = \sum_j^{L_m} \sqrt{\sum_i^{P} \{[(\mathbf{AD}_h)_{ij}]^2 + [(\mathbf{AD}_v)_{ij}]^2\}}, \tag{5}$$

where $\mathbf{D}_h \in R^{L_m \times L_m}$ and $\mathbf{D}_v \in R^{L_m \times L_m}$ denote the differences operation in the horizontal and vertical direction, respectively. The introduced formulation (5) can impose sparsity in the distribution of the absolute gradient of the abundance.

Furthermore, note that the abundance coefficient vectors contain only a few non-zero values since only a subset of the available endmembers will contribute to the spectrum of a single pixel. So the abundance matrix $\mathbf{A}$ should be sparse too. We propose using the convex sparse regularization l_1 norm to impose sparsity on $\mathbf{A}$, which can be expressed as $\|\mathbf{A}\|_1$. The associated optimization problem becomes:

$$\min_{\mathbf{A}} \|\mathbf{Y}_h - \mathbf{EAHD}\|_F^2 + \|\mathbf{Y}_m - \mathbf{REA}\|_F^2 + \mu \mathrm{TV}(\mathbf{A}) + \alpha_a \|\mathbf{A}\|_1. \tag{6}$$

where μ, α_a are the regularization parameters for total variation and sparse representation, respectively.

2.2.3. *blur kernel regularization*

Various blur kernel priors have been proposed, such as Laplacian operator, simultaneous-autoregression et al. In this paper, considering the smoothness of the blur kernel, we propose the following total variation regularization for blur kernel:

$$\mathrm{TV}(\mathbf{H}) = \|\mathbf{HD}_h\|_F^2 + \|\mathbf{HD}_v\|_F^2. \tag{7}$$

2.2.4. *unifying objective function*

By combining (6) and (7), we have a unifying objective function described as:

$$\min_{\mathbf{A},\mathbf{H}} \|\mathbf{Y}_h - \mathbf{EAHD}\|_F^2 + \|\mathbf{Y}_m - \mathbf{REA}\|_F^2 + \mu \mathrm{TV}(\mathbf{A}) + \alpha_a \|\mathbf{A}\|_1 + \alpha_h \mathrm{TV}(\mathbf{H}). \tag{8}$$

where α_h is regularization parameter for the blur kernel. Our estimation method for blind HSI super resolution is to solve the unifying optimization formulation (8). It is seen that (8) combines the blur kernel and image estimation together. By contrast, in [18], the authors separated the blur kernel and HSI estimation so that the image estimation error is magnified.

3. OPTIMIZATION ALGORITHM

To solve effectively (6), we use the block coordinate descent method [21] to decompose the problem (8) into the following two sub-problems:

$$(P1) \quad \min_{\mathbf{A}} \|\mathbf{Y}_h - \mathbf{EAHD}\|_F^2 + \|\mathbf{Y}_m - \mathbf{REA}\|_F^2 + \mu \mathrm{TV}(\mathbf{A}) + \alpha_a \|\mathbf{A}\|_1$$

$$(P2) \quad \min_{\mathbf{H}} \|\mathbf{Y}_h - \mathbf{EAHD}\|_F^2 + \alpha_h \mathrm{TV}(\mathbf{H}).$$

By ADMM [22] and introducing new variations $\mathbf{V}_1 = \mathbf{EA}, \mathbf{V}_2 = \mathbf{A}, \mathbf{V}_3 = \mathbf{AD}_h, \mathbf{V}_4 = \mathbf{AD}_v, \mathbf{V}_5 = \mathbf{A}$, the augmented Lagrangian function for $P1$ is given by:

$$
\begin{aligned}
&L_1(\mathbf{A},\mathbf{V}_1,\mathbf{V}_2,\mathbf{V}_3,\mathbf{V}_4,\mathbf{V}_5)\\
&=\|\mathbf{Y}_h-\mathbf{E}\mathbf{V}_1\mathbf{D}\|_F^2+\|\mathbf{Y}_m-\mathbf{R}\mathbf{E}\mathbf{V}_2\|_F^2\\
&+\frac{\lambda_1}{2}\|\mathbf{V}_1-\mathbf{A}\mathbf{H}-\mathbf{D}_1\|_F^2+\frac{\lambda_1}{2}\|\mathbf{V}_2-\mathbf{A}-\mathbf{D}_2\|\\
&+\frac{\lambda_1}{2}\|\mathbf{V}_3-\mathbf{A}\mathbf{D}_h-\mathbf{D}_3\|_F^2+\frac{\lambda_1}{2}\|\mathbf{V}_4-\mathbf{A}\mathbf{D}_v-\mathbf{D}_4\|_F^2\\
&+\frac{\mu}{2}\mathrm{TV}(\mathbf{V}_3,\mathbf{V}_4)+\alpha_a\|\mathbf{V}_5\|_1+\frac{\lambda_1}{2}\|\mathbf{V}_5-\mathbf{A}-\mathbf{D}_5\|_F^2,
\end{aligned}
\tag{9}
$$

where $\mathbf{D}_1,\mathbf{D}_2,\mathbf{D}_3,\mathbf{D}_4,\mathbf{D}_5$ are dual variables, λ_1 is penalty parameter.

By introducing $\mathbf{Z}=\mathbf{H}\mathbf{D}$, the augmented Lagrangian function for $P2$ is given by:

$$
\begin{aligned}
L_2(\mathbf{H},\mathbf{Z})=\|\mathbf{Y}_h-\mathbf{E}\mathbf{A}\mathbf{Z}\|_F^2+\lambda_2\|\mathbf{Z}-\mathbf{H}\mathbf{D}-\mathbf{U}\|_F^2\\
+\alpha_h(\|\mathbf{H}\mathbf{D}_h\|_F^2+\|\mathbf{H}\mathbf{D}_v\|_F^2).
\end{aligned}
\tag{10}
$$

where $\mathbf{U}$ is a dual variable, λ_2 is a penalty parameter. We first illustrate how to solve the two subproblems in the follow steps.

1) Minimizing L_1 for $\mathbf{A}$, given the other variables

It is the least squares problem and thus the solver is given by:

$$
\begin{aligned}
\mathbf{A}^{k+1}=((\mathbf{V}_1-\mathbf{D}_1)\mathbf{H}^T+(\mathbf{V}_2-\mathbf{D}_2)+(\mathbf{V}_3-\mathbf{D}_3)\mathbf{D}_h^T\\
+(\mathbf{V}_4-\mathbf{D}_4)\mathbf{D}_v^T+(\mathbf{V}_5-\mathbf{D}_5))(\mathbf{H}\mathbf{H}^T+\mathbf{D}_h\mathbf{D}_h^T\\
+\mathbf{D}_v\mathbf{D}_v^T+2I)^{-1}
\end{aligned}
\tag{11}
$$

2) Minimizing L_1 for $\mathbf{V}_1$, given the other variables

Similar to step 1), the solver is given by:

$$
\begin{aligned}
&\mathbf{V}_1^{k+1}(:,\delta)=(\mathbf{E}^T\mathbf{E}+\mathbf{I})^{-1}(\mathbf{E}^T\mathbf{Y}_h+(\mathbf{A}^{k+1}\mathbf{H}-\mathbf{D}_1)(:,\delta))\\
&\mathbf{V}_1^{k+1}(:,1-\delta)=(\mathbf{A}^{k+1}\mathbf{H}-\mathbf{D}_1)(:,1-\delta)\\
&\mathbf{D}_1^{k+1}=\mathbf{D}_1^k-(\mathbf{V}_1^{k+1}-\mathbf{A}^{k+1}\mathbf{H}).
\end{aligned}
\tag{12}
$$

where $\delta\in\{0,1\}^{PN_m}$ and $\delta(i)=1$ when the position i is sampled and the other is 0.

3) Minimizing L_1 for $\mathbf{V}_2$, given the other variables

Similar to step 1), the solver is given by:

$$
\begin{aligned}
&\mathbf{V}_2^{k+1}=((\mathbf{R}\mathbf{E})^T\mathbf{R}\mathbf{E}+\lambda_1\mathbf{I})^{-1}(\mathbf{A}^{k+1}+\mathbf{D}_2+(\mathbf{R}\mathbf{E})^T\mathbf{Y}_m)\\
&\mathbf{D}_2^{k+1}=\mathbf{D}_2^k-(\mathbf{V}_2^{k+1}-\mathbf{A}^{k+1}).
\end{aligned}
\tag{13}
$$

4) Minimizing L_1 for $\mathbf{V}_3,\mathbf{V}_4$, given the other variables

By using vector-soft threshold method [3] ,the solver is given by:

$$
\begin{aligned}
&\{(\mathbf{V}_3^{k+1})_{:,j},(\mathbf{V}_4^{k+1})_{:,j}\}=\max\{\|\mathbf{C}\|_F-\frac{\mu}{\lambda_2},0\}\frac{\mathbf{C}}{\|\mathbf{C}\|_F},\\
&\mathbf{D}_3^{k+1}=\mathbf{D}_3^k-(\mathbf{A}^{k+1}\mathbf{D}_h-\mathbf{V}_3^{k+1})\\
&\mathbf{D}_4^{k+1}=\mathbf{D}_4^k-(\mathbf{A}^{k+1}\mathbf{D}_v-\mathbf{V}_4^{k+1}).
\end{aligned}
\tag{14}
$$

where $\mathbf{C}=\{(\mathbf{A}^{k+1}\mathbf{D}_h-\mathbf{D}_3^k)_{:,j},(\mathbf{A}^{k+1}\mathbf{D}_v-\mathbf{D}_4^k)_{:,j}\}$ $(:,j)$ denotes the jth collum of the matrix.

5) Minimizing L_1 for $\mathbf{V}_5$, given the other variables

Similar to step 4), the solver is given by:

$$
\begin{aligned}
&\mathbf{V}_5=\mathrm{sign}(\mathbf{A}^{k+1}-\mathbf{D}_5^k)\times\max\{\mathbf{0},|\mathbf{V}_5|-\frac{2\alpha_a}{\lambda_1}\}.\\
&\mathbf{D}_5^{k+1}=\mathbf{D}_5^k-(\mathbf{V}_5^{k+1}-\mathbf{A}^{k+1}).
\end{aligned}
\tag{15}
$$

6) Minimizing L_2 for $\mathbf{H}$, given the other variables

The solver is given by:

$$
\begin{aligned}
\mathbf{H}^{k+1}=\lambda_2(\mathbf{Z}-\mathbf{U})\mathbf{D}^T(\lambda_2(\mathbf{D}_h\mathbf{D}_h^T+\mathbf{D}_v\mathbf{D}_v^T)\\
+\alpha_h\mathbf{D}\mathbf{D}^T)^{-1}.
\end{aligned}
\tag{16}
$$

7) Minimizing L_2 for $\mathbf{Z}$, given the other variables

the solver is given by:

$$
\begin{aligned}
&\mathbf{Z}^{t+1}=((\mathbf{E}\mathbf{A}^{k+1})^T(\mathbf{E}\mathbf{A}^{k+1})+\lambda_2I)^{-1}((\mathbf{E}\mathbf{A}^{k+1})^T\mathbf{Y}_h\\
&\qquad+\lambda_2(\mathbf{H}\mathbf{D}+\mathbf{U}))\\
&\mathbf{U}^{k+1}=\mathbf{U}^k-(\mathbf{Z}^{k+1}-\mathbf{H}^{k+1}\mathbf{D}).
\end{aligned}
\tag{17}
$$

Now, the proposed algorithm implementation is listed in Algorithm 1.

Algorithm 1 Blind HS image super resolution algorithm

1: Input: $\mathbf{Y}_m,\mathbf{Y}_h$
2: Output: $\widehat{\mathbf{Y}}$
3: estimate $\mathbf{E}$ according to VCA
4: initial $\mathbf{H}^0,\mathbf{V}_1^0\sim\mathbf{V}_5^0,\mathbf{U}^0,\mathbf{D}_1^0\sim\mathbf{D}_5^0$
5: **repeat**
6: update $\mathbf{A}^{k+1}$ according to (11)
7: update $\mathbf{V}_1^{k+1}$ and $\mathbf{D}_1^{k+1}$ according to (12)
8: update $\mathbf{V}_2^{k+1}$ and $\mathbf{D}_2^{k+1}$ according to (13)
9: update $\mathbf{V}_3^{k+1},\mathbf{V}_4^{k+1},\mathbf{D}_3^{k+1},\mathbf{D}_4^{k+1}$ according to (14)
10: update $\mathbf{V}_5^{k+1}$ and $\mathbf{D}_5^{k+1}$ according to (15)
11: update $\mathbf{H}^{k+1}$ according to (16)
12: update $\mathbf{Z}^{k+1}$ and $\mathbf{U}^{k+1}$ according to (17)
13: **until** stopping criteria are satisfied
14: set $\widehat{\mathbf{Y}}=\mathbf{E}\mathbf{A}^{k+1}$.

4. EXPERIMENTAL RESULT

We compare the proposed method with the HySure method [18], based on two real hyperspectral image datasets. One is Pavia University, which is reduced to 93 bands after removing the water vapor absorption bands with 128×128 pixels of every band. Another is Paris dataset, which was obtained by the Earth Observing-1 satellite. We generate the low spatial resolution HSI by blurring the reference image and downsampling with sampling ratio 4. The spectral response of the IKONOS satellite is used as spectral response to generate the MSI. For our experiments, we select a 5×5 exponential blur kernel and a 5×5 uniform blur kernel. Furthermore, we add Gaussian noise with SNR 25db for HSI and MSI.

By testing a wide range of values of these parameters, we set $\lambda_1 = 1$, $\lambda_2 = 2$, $\mu = 0.05$, $\alpha_a = 0.01$, and $\alpha_h = 0.5$ for the highest quality performance. Since there are several hundred bands in HSI, we only show a composite false color result like the HySure method by selecting the red, green, and blue bands. By selecting bands 40, 22, 7, the composite image of the reconstruction results and the local details of our method and HySure method for the Pavia university dataset are shown in Fig.1. Furthermore, Table 1 shows the quality indices, which are peak signal-to-noise ratio (PSNR), root mean square error (RMSE), universal image equality index (UIQI), spectral angle mapper (SAM), relative dimensionless global error in synthesis (ERGAS), degree of distortion (DD).

With the same blur kernel and noise intensity the composite false color reconstruction result and the local details for Paris dataset (bands [45, 30, 10]) are shown in Fig.2. Table 2 gives the performance evaluation correspondingly. From these results we see that our method preserves a clear detail structure and edge information.

Table 1. performance of two methods(Pavia dataset : psnr(db), rmse(in 10^{-2}), uiqi, sam(in degree), ergas and dd(in 10^{-3}).

method	Exponential blur kernel					
	PSNR	RMSE	UIQI	SAM	ERGAS	DD
HySure	34.112	1.701	0.969	2.606	1.559	1.218
Proposed	**35.337**	**1.476**	**0.979**	**2.225**	**1.315**	**1.118**
method	Uniform blur kernel					
	PSNR	RMSE	UIQI	SAM	ERGAS	DD
HySure	34.189	1.697	0.970	2.541	1.524	1.103
Proposed	**35.415**	**1.423**	**0.980**	**2.163**	**1.209**	**1.053**

Table 2. performance of two methods(Paris dataset : psnr(db), rmse(in 10^{-2}), uiqi, sam(in degree), ergas and dd(in 10^{-3}).

method	Exponential blur kernel					
	PSNR	RMSE	UIQI	SAM	ERGAS	DD
HySure	35.562	2.140	0.901	2.782	2.957	1.502
Proposed	**37.868**	**1.641**	**0.931**	**2.178**	**2.254**	**1.131**
method	Uniform blur kernel					
	PSNR	RMSE	UIQI	SAM	ERGAS	DD
HySure	35.289	2.220	0.900	2.901	3.024	1.540
Proposed	**37.681**	**1.733**	**0.930**	**2.183**	**2.302**	**1.154**

Furthermore, we compare the blur kernel estimation error by computing the l_2 norm of difference between the true kernel and estimated kernel. Table 3 lists the estimation error. From the Table 3 we observe that our method obtains more accurate estimated blur kernel than HySure method.

Fig. 1. Result of the two methods on Pavia dataset. (a) True HS image. (b) Nearest-neighbor interpolation of observed HS image. (c) HySure method. (d) Proposed method. (e-h) are the corresponding magnified details.

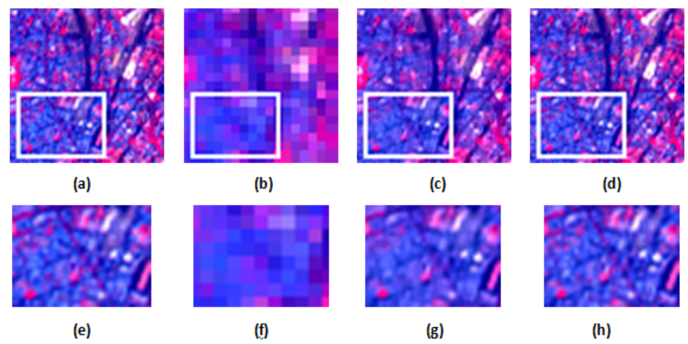

Fig. 2. Result of the two methods on Paris dataset. (a) True HS image. (b) Nearest-neighbor interpolation of observed HS image. (c) HySure method. (d) Proposed method. (e-h) are the corresponding magnified details.

Table 3. blur kernel estimation error of two methods.

method	Exponential blur kernel			Uniform blur kernel		
	5×5	7×7	9×9	5×5	7×7	9×9
HySure	0.0057	0.0084	0.012	0.0061	0.0087	0.019
Proposed	**0.0043**	**0.0068**	**0.009**	**0.0045**	**0.0071**	**0.013**

5. CONCLUSION

This paper has proposed a novel method for blind HSI super resolution based on linear spectral unmixing model. The proposed method can estimate simultaneously the unknown hyperspectral image and the blur kernel based on the linear spectral unmixing technique. The TV term is used for the blur regularization and the sparse representation and TV are used for abundance regularization terms. Because the image and blur kernel are simultaneously estimated, the estimation error can be minimized so that the performance of the proposed method can be improved. Experimental results show that the proposed method is superior to HySure method in terms of reconstruction quality.

6. REFERENCES

[1] Y. Gu, Y. Zheng, and J. Zhang, “Integration of spatial-spectral information for resolution enhancement in hyperspectral images,” IEEE Trans. Geosci. Remote Sens., vol. 46, no. 5, pp. 1347-1357, May 2008.

[2] F. Palsson, J. R. Sveinsson, M. O. Ulfarsson, and J. A. Benediktsson, “Model-based fusion of multi- and hyperspectral images using PCA and wavelets,” IEEE Trans. Geosci. Remote Sens., vol. 53, no. 5, pp. 2652-2663, May 2015.

[3] C. Grohnfeldt, X. Zhu, and R. Bamler, “Jointly sparse fusion of hyperspectral and multispectral imagery,” in Proc. IEEE Int. Geosci. Remote Sens. Symp., Melbourne, Australia, Jul. 2013, pp. 4090-4093.

[4] R. C. Hardie, M. T. Eismann, and G.L. Wilson, “MAP estimation for hyperspectral image resolution enhancement using an auxiliary sensor,” IEEE Trans. Image Processing., vol. 13, no. 9, pp. 1174-1184, Mar. 2004.

[5] Y. Zhang, S. D. Backer, and P. Scheunders, “Noise-resistant wavelet-based Bayesian fusion of multispectral and hyperspectral images,” IEEE Trans. Geosci. Remote Sens., vol. 47, no. 11, pp. 3834-3843, Nov. 2009.

[6] N. Akhtar, F. Shafait and A. Mian, “Bayesian Sparse Representation for Hyperspectral Image Super Resolution,” IEEE Conf. on Computer Vision and Pattern Recognition, 2015, pp. 3631-3640.

[7] Q. Wei, N. Dobigeon, and J. Y. Tourneret, “Bayesian fusion of multi-band images,” IEEE J. Sel. Topics Signal Process., vol. 9, no. 6, pp. 1-11, Sep. 2015.

[8] B. Lin, X. Tao, S. Li, L. Dong, and J. Lu, “Variational Bayesian image fusion based on combined sparse representations,” In: IEEE Int. Conf.Acoustics, Speech and Signal Processing, 2016, pp. 1432-1436.

[9] N. Yokoya, T. Yairi, and A. Iwasaki, “Coupled nonnegative matrix factorization unmixing for hyperspectral and multispectral data fusion,” IEEE Trans. Geosci. Remote Sens., vol. 50, no. 2, pp. 528-537, Feb. 2012.

[10] R. Kawakami, J. Wright, Y. W. Tai, Y. Matsushita, M. Ben-Ezra, and K. Ikeuchi,“High-resolution hyperspectral imaging via matrix factorization,” IEEE Conf. on Computer Vision and Pattern Recognition, 2011, pp. 2329-2336.

[11] E. Wycoff, T. H. Chan, K. Jia, W. K. Ma, and Y. Ma, “A non-negative sparse promoting algorithm for high resolution hyperspectral imaging,” In: IEEE Int. Conf.Acoustics, Speech and Signal Processing, 2013, pp. 1409-1413.

[12] B. Huang, H. Song, H. Cui, J. Peng, and Z. Xu, “Spatial and spectral image fusion using sparse matrix factorization,” IEEE Trans. Geosci. Remote Sens. vol. 52, no. 3, pp. 1693-1704, Mar. 2014.

[13] N. Akhtar, F. Shafait, and A. Mian, “Sparse spatio-spectral representation for hyperspectral image super-resolution,” ECCV, Lecture Notes in Computer Science, 2014, vol. 8695, pp. 63-78.

[14] C. Lanaras, E. Baltsavias, and K. Schindler, “Hyperspectral super-resolution by coupled spectral unmixing,” in Proc. IEEE Int. Conf. on Computer Vision, Dec. 2015, pp. 3586-3594.

[15] M. Bendoumi, M. He, and S. Mei, “Hyperspectral image resolution enhancement using high-resolution multispectral image based on spectral unmixing” IEEE Trans. Geosci. Remote Sens. vol. 52, no. 10, pp. 6574-6583, Oct. 2014.

[16] Q. Wei, J. Bioucas-Dias, N. Dobigeon and J. Y. Tourneret, “Hyperspectral and multispectral image fusion based on a sparse representation,” IEEE Trans. Geosci. and Remote Sens., vol. 53, no. 7, pp. 3658-3668, Jul. 2015.

[17] W. Dong, F. Fu, G. Shi, X. Cao, J. Wu, G. Li, and X. Li, “Hyperspectral image super-resolution via non-negative structured sparse representation” IEEE Trans. image process. vol. 5, no. 25, pp. 2337-2352, May, 2016.

[18] M. Simoes, J. Bioucas-Dias, L. B. Almeida, and J. Chanussot, “A convex formulation for hyperspectral image super resolution via subspace-based regularization,” IEEE Trans. Geosci.Remote Sens., vol. 53, no. 6, pp. 3373-3388, Jun. 2015.

[19] J. Bioucas-Dias, A. Plaza, N. Dobigeon, M. Parente, Q. Du, P. Gader, and J. Chanussot, “Hyperspectral unmixing overview: Geometrical,statistical, and sparse regression-based approaches,” IEEE J. Sel. Topics Appl. Earth Observ. and Remote Sens., vol. 5, no. 2, pp. 354-379, Apr. 2012.

[20] J. Nascimento and J. Bioucas-Dias, “Vertex component analysis: A fast algorithm to unmix hyperspectral data,” IEEE Trans. Geosci. Remote Sens., vol. 43, no. 4, pp. 898-910, 2005.

[21] D. P. Bertsekas, Nonlinear programming. Athena Scientific, 1999.

[22] S. Boyd, N. Parikh, E. Chu, B. Peleato, and J. Eckstein, “Distributed optimization and statistical learning via the alternating direction method of multipliers,” Foundations and Trends in Machine Learning, vol. 3, no. 1, pp. 1-122, 2010.